Supporting Information

Exploring the Role of the Third Active Site Metal Ion in DNA Polymerase η with QM/MM Free Energy Simulations

David R. Stevens and Sharon Hammes-Schiffer*

Department of Chemistry, Yale University, 225 Prospect Street, New Haven, Connecticut 06520

Corresponding author: sharon.hammes-schiffer@yale.edu

TABLE OF CONTENTS

Methods

Preparation and equilibration of the systems

The system with two metal ions in the active site was based on the reactant crystal structure PDB ID: 3MR2 and the product crystal structure PDB ID: 4ECS.[1-2] For the reactant, the missing residues were added using the protein preparation module from the Maestro program,[3] and the hydrogen atoms were added using the H++ program.[4] Then the reactant system was solvated in TIP3P water[5] with 0.15 M NaCl. The solvent and ions were equilibrated with the protein/DNA system fixed by first minimizing the energy using the steepest descent algorithm for 5000 steps, followed by 500 ps NVT molecular dynamics and then 500 ps NPT molecular dynamics at 300 K. This solvated system was used as the initial reactant structure for the QM/MM string simulations. For the initial product structure, the active site of the product crystal structure was superimposed on this initial solvated reactant structure using the Maestro program.[3] Thus, the initial reactant and product structures were identical except for the active site, which was defined as the QM region in Figure 1 of the main paper. The system with three metal ions in the active site was based on the reactant and product structures contained in PDB ID: 4ECV,[2] and the initial reactant and initial product structures were obtained in the same way as for the system with two metal ions using the alternative positions for the product contained in the PDB file.

The molecular mechanical (MM) simulations utilized the AMBER ff14SB force field[6-10] for the protein and DNA in conjunction with the TIP3P water model. The parameters for the pyrophosphate (OPP/PPi) were obtained from a previous study,[11] and the parameters for dATP were obtained from previous simulations of the Pol η system.[12] The equilibration was performed with the Amber program.[13-14]

QM/MM free energy simulations

The QM/MM free energy simulations were performed using a CHARMM[15]/Q-Chem[16] interface.[17] Prior to the QM/MM simulations, the system was truncated by deleting all water molecules and ions more than 15 Å from any nucleic acid or protein atom. The MM region was treated as described above for the equilibration. The QM region was treated with density functional theory (DFT) using the B3LYP functional[18-19] and the 6-31G** basis set. Hydrogen

capping was used to treat the boundary between the QM and MM regions. For the QM/MM simulations, residues more than 18 Å from the active site Mg^{2+} ion in the B position were kept fixed.

We used the initial reactant and product structures described above to generate the initial strings for the sequential mechanism, corresponding to phosphoryl transfer followed by proton transfer, as well as the concerted mechanism for both the two-metal and three-metal systems. First the geometry of the QM region was optimized for the initial reactant and product structures at the QM/MM level with the rest of the system fixed. This product structure corresponded to only the phosphoryl transfer reaction and is denoted as the intermediate product structure. The final product structure was obtained by manually moving the proton from the O3' of the dATP to the O2B atom of the leaving group, as illustrated in Figure 2 of the main paper, followed by optimization of the QM region at the QM/MM level with the O2B-H3T bond restrained with a 500 kcal/(mol•$Å^2$) force constant.

These partially optimized reactant, intermediate product, and final product structures are identical except for the QM region, and the initial strings were obtained by interpolating between the QM regions of these structures. The initial string corresponding to the concerted mechanism was obtained through linear interpolation between the reactant structure and the final product structure. The initial string corresponding to the sequential mechanism was obtained through linear interpolation between the reactant structure and the intermediate product structure, as well as linear interpolation between the intermediate product structure and the final product structure. The concerted and sequential initial strings were obtained in this manner for both the two-metal and the three-metal systems.

The finite temperature string method with umbrella sampling is described in detail elsewhere.[20-23] In this approach, the string is represented by a set of images, and each image is associated with a set of reaction coordinate values used in the umbrella sampling restraints. We performed four independent string simulations corresponding to the two different initial strings (i.e., the concerted and sequential mechanisms) for the two-metal and three-metal systems. Eleven and fifteen reaction coordinates were used for the two-metal and three-metal systems, respectively, as shown in Figure S1. The sequential mechanism was simulated with 30 images along the string for both the two-metal and three-metal systems. The concerted mechanism was simulated with 20 and 15 images for the two-metal and three-metal systems, respectively. For each image along the

string, the MM region was equilibrated for 10 ps while keeping the QM region fixed, and then the full system was equilibrated for 100 fs.

In these string simulations, an iterative procedure that involves updating the reaction coordinate values used in the umbrella sampling restraints was performed until convergence. For each iteration, a 100 fs molecular dynamics (MD) trajectory was propagated for each image. For the two-metal system, 29 iterations were performed for both independent string simulations, and for the three-metal system, 25 and 30 iterations were performed for the string simulations based on the sequential and concerted initial strings, respectively. Thus, the total amount of MD sampling was 145 ps for the two-metal system and 120 ps for the three-metal system. The convergence of the strings was determined from the root-mean-square deviations (RMSDs) of the reaction coordinates[23] and the free energy profiles, as illustrated in Figures S5 and S6. The multidimensional free energy surfaces were obtained from all of the data within a given string simulation using the binless[20, 24] weighted histogram analysis method (WHAM). Thus, the free energy is computed as a function of all 11 or 15 reaction coordinates for the two-metal or three-metal system, respectively, as defined in Figure S1. Then the data are projected onto a two-dimensional surface defined by two key combined coordinates: the phosphoryl transfer coordinate (R1 – R2) and the proton transfer coordinate (R3 – R4). The resulting two-dimensional free energy surfaces shown in Figure 3 of the paper are averaged over all other reaction coordinates. The final converged string is the minimum free energy path (MFEP), and the free energy along the MFEP is plotted in the insets of Figure 3 of the main paper.

QM/MM MD trajectories

To investigate the possibility of a hydroxide ion bound to Mg_A^{2+} as the base deprotonating 3'OH, we propagated additional QM/MM MD trajectories for both the two- and three-metal systems using the same methodology as described above with the CHARMM/Q-Chem interface. The trajectories were started from the last configuration of the sixth image along the string for the final iteration. To create the Mg^{2+}-bound hydroxide, a hydrogen was deleted from the water bound to the Mg^{2+} in the A position (M_A in Figure S1), and a hydrogen was appended to the attacking O3' in the reactant state, followed by 50 steps of steepest descent geometry optimization of only this hydrogen on 3'OH. The MD trajectories were then propagated for 200 ps and 500 ps for the two- and three-metal systems, respectively.

For the two-metal system, the proton transferred from the 3'OH to the Mg^{2+}-bound hydroxide and stayed there for the remainder of the trajectory. The same procedure was performed starting with configurations from the eighth image along the string and led to similar results. However, when the same procedure was performed starting with configurations from the second image along the string, the proton transferred to the Mg^{2+}-bound hydroxide and then transferred back to the O3' and remained there. These results suggest that the pK_a of the 3'OH is greater than the pK_a of the Mg^{2+}-bound water for the initial images of the string, but the pK_a of the 3'OH decreases as it attacked the phosphate, thereby allowing it to transfer its proton to the Mg^{2+}-bound hydroxide. For the three-metal system, the proton transferred from a water molecule coordinated to the Mg^{2+} ion in the C position to the Mg_A^{2+}-bound hydroxide, and the 3'OH was not deprotonated. This result suggests that the Mg^{2+}-bound hydroxide would need to deprotonate the 3'OH prior to the arrival of the third Mg^{2+} ion in the active site.

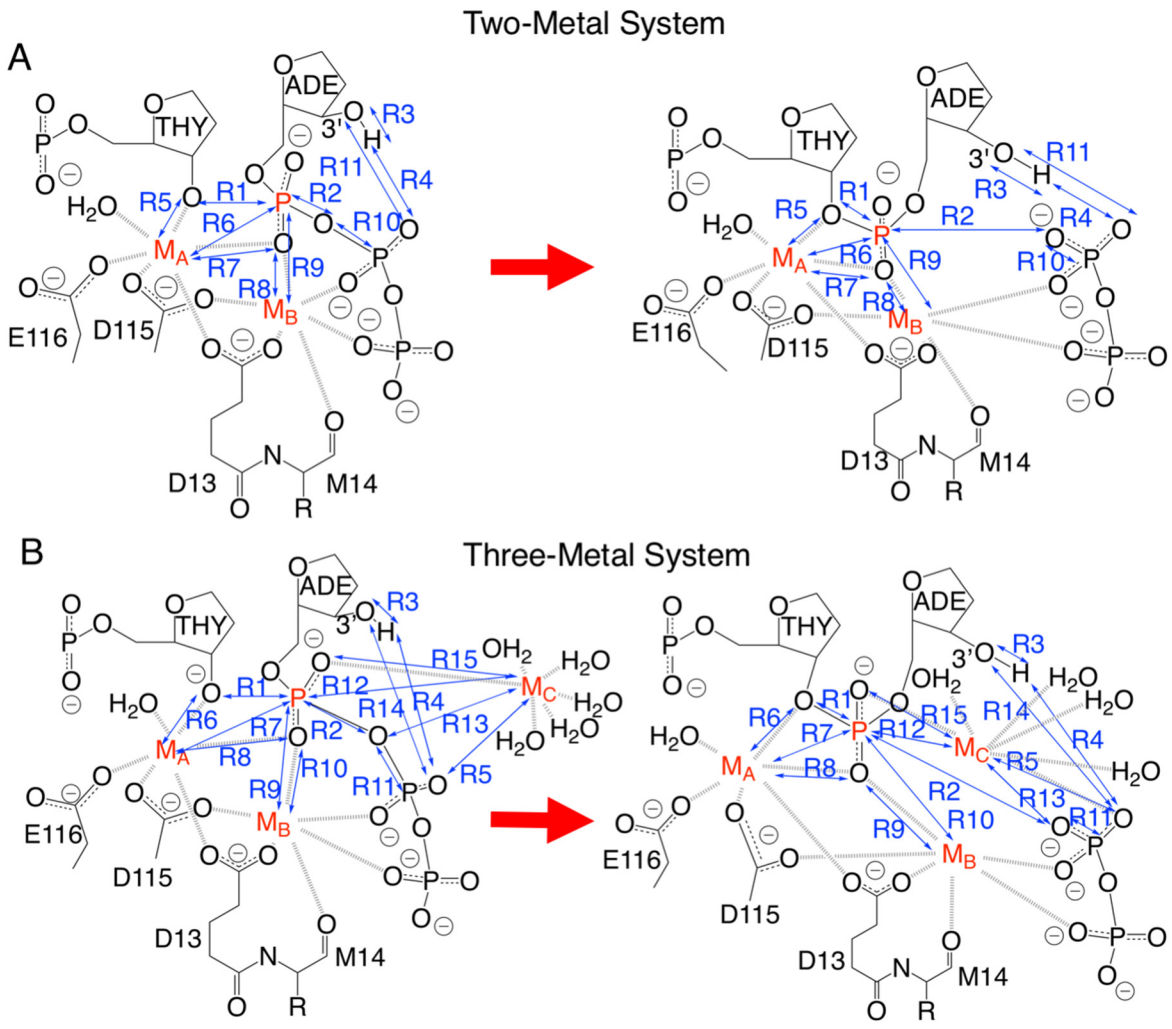

Figure S1. Reaction coordinates used in the QM/MM free energy simulations for (A) the two-metal system, which used 11 reaction coordinates and (B) the three-metal system, which used 15 reaction coordinates. Note that the numbering of the reaction coordinates in this figure is different from that used in Figure 1 of the main paper. Moreover, the water that is no longer coordinated to M_C in the product of the three-metal system is omitted for visual clarity.

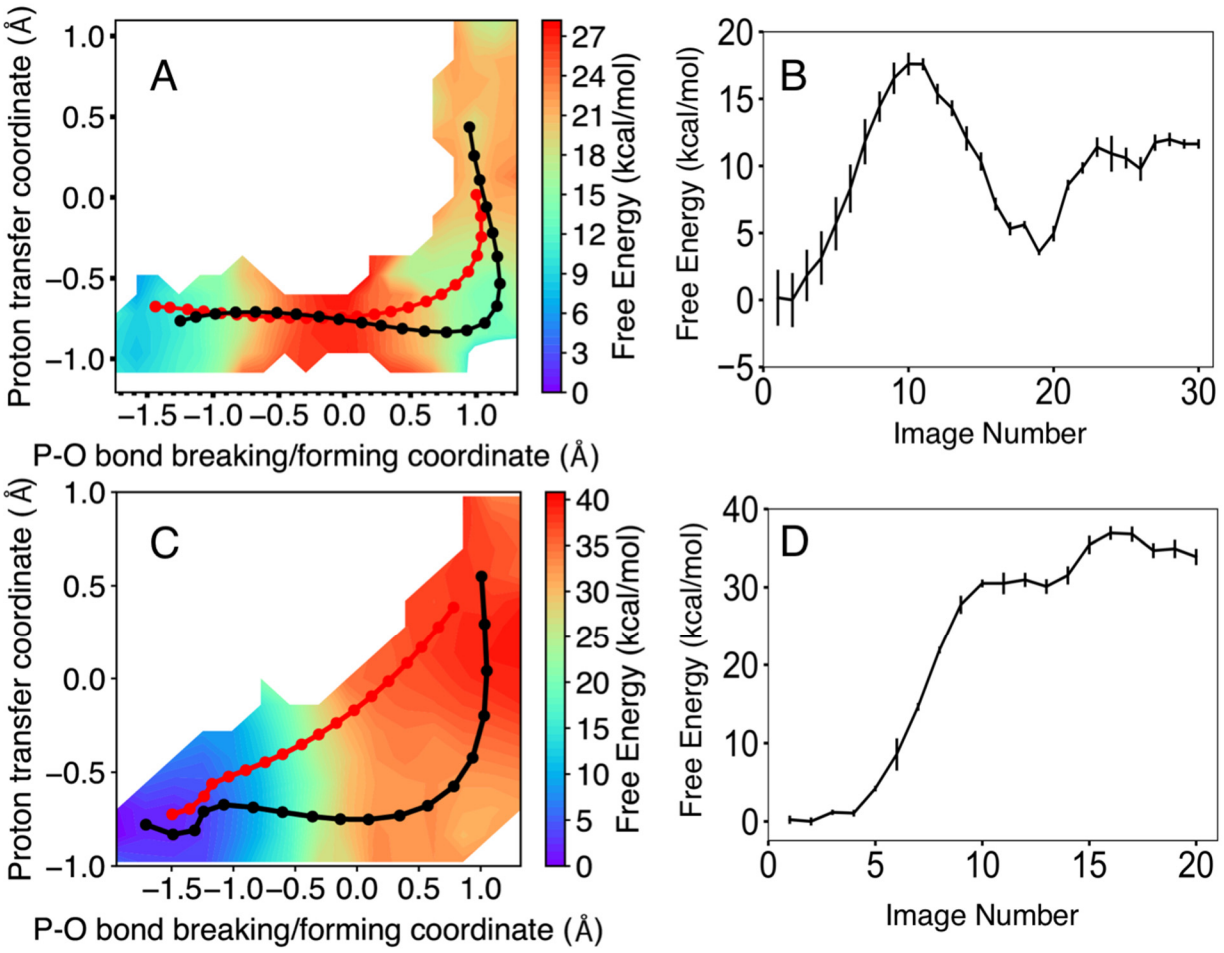

Figure S2: Two-dimensional free energy surface as a function of the proton transfer coordinate and the P–O bond breaking/forming coordinate for two independent string simulations of the Pol η system with two metal ions in the active site. In parts (A) and (C), the initial string for each independent string simulation is shown in red, and the final string is shown in black, with the images along the string depicted as red or black circles, respectively. In parts (B) and (D), the free energy along the MFEP in parts (A) and (C), respectively, is plotted as a function of evenly spaced images. The initial string corresponds to a sequential mechanism, where phosphoryl transfer occurs prior to proton transfer, in (A) and to a concerted mechanism, where both steps occur simultaneously, in (C). Both string simulations converged to the sequential mechanism, where phosphoryl transfer occurs prior to proton transfer. The first independent string was determined to be better converged because the initial string was closer to the final string, and therefore it sampled the intermediate product region more extensively. Thus, the first string is shown in the main paper. The error bars in the free energy profiles along the MFEP correspond to the statistical errors of the WHAM procedure and were obtained using a bootstrapping error analysis with nine "fake" data sets.[25] Note that these error bars do not account for errors arising from the level of theory used to generate the potential energy surface and the limited conformational sampling, resulting in potentially misleading smaller statistical error bars for the second independent string.

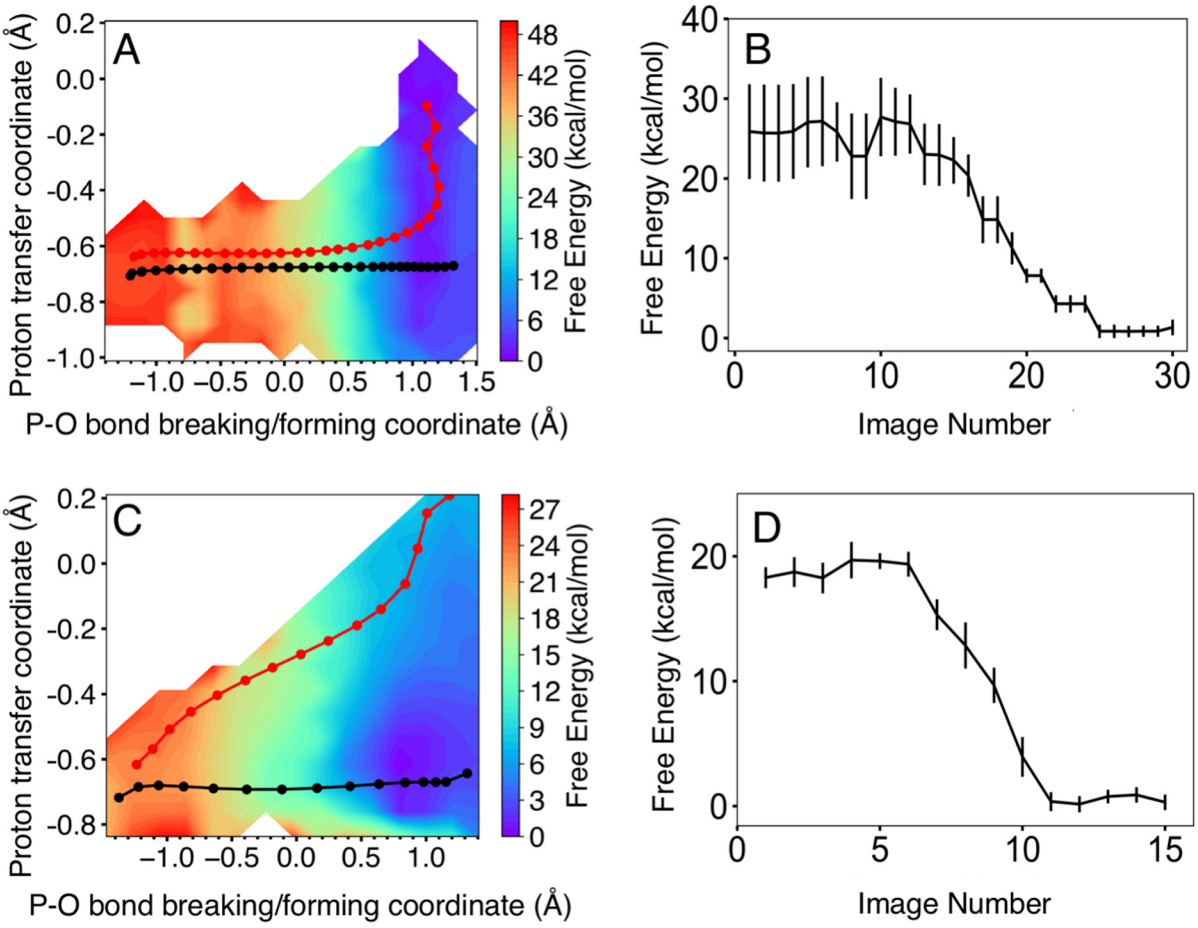

Figure S3: Two-dimensional free energy surface as a function of the proton transfer coordinate and the P–O bond breaking/forming coordinate for two independent string simulations of the Pol η system with three metal ions in the active site. In parts (A) and (C), the initial string for each independent string simulation is shown in red, and the final string is shown in black, with the images along the string depicted as red or black circles, respectively. In parts (B) and (D), the free energy along the MFEP in parts (A) and (C), respectively, is plotted as a function of evenly spaced images. The initial string corresponds to a sequential mechanism, where phosphoryl transfer occurs prior to proton transfer, in (A) and to a concerted mechanism, where both steps occur simultaneously, in (C). Both string simulations converged to the same mechanism, which corresponds to only phosphoryl transfer with no subsequent proton transfer. The second independent string was determined to be better converged and therefore is shown in the main paper. The error bars in the free energy profiles along the MFEP correspond to the statistical errors of the WHAM procedure and were obtained using a bootstrapping error analysis with nine "fake" data sets.[25] Note that these error bars do not account for errors arising from the level of theory used to generate the potential energy surface and the limited conformational sampling.

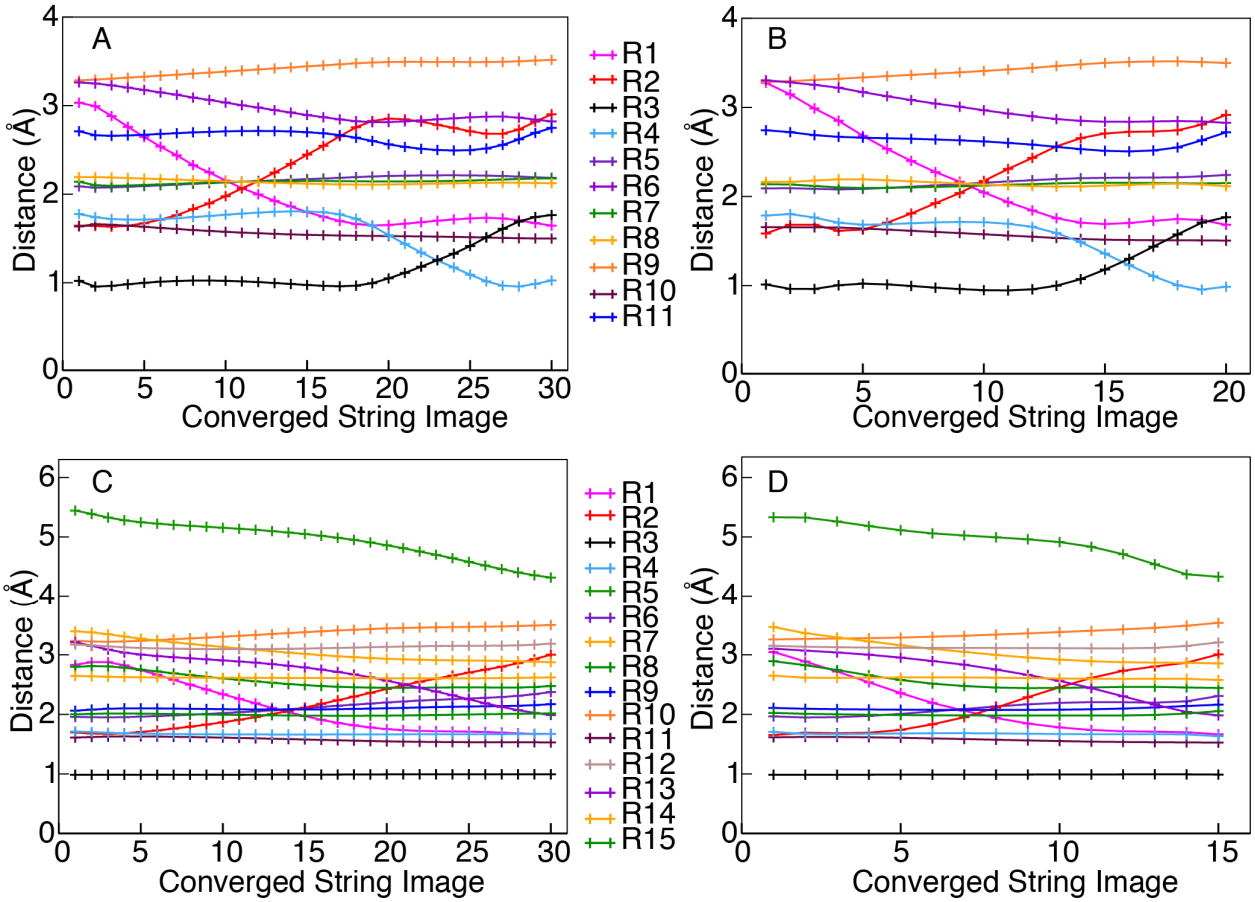

Figure S4: Plots of all reaction coordinates (defined in Figure S1) along the MFEPs for the Pol η system with two metal ions in the active site for parts (A) and (B) and three metal ions in the active site for parts (C) and (D). Parts (A) and (B) correspond to Figures S2A and S2C, respectively, and parts (C) and (D) correspond to Figures S3A and S3C, respectively.

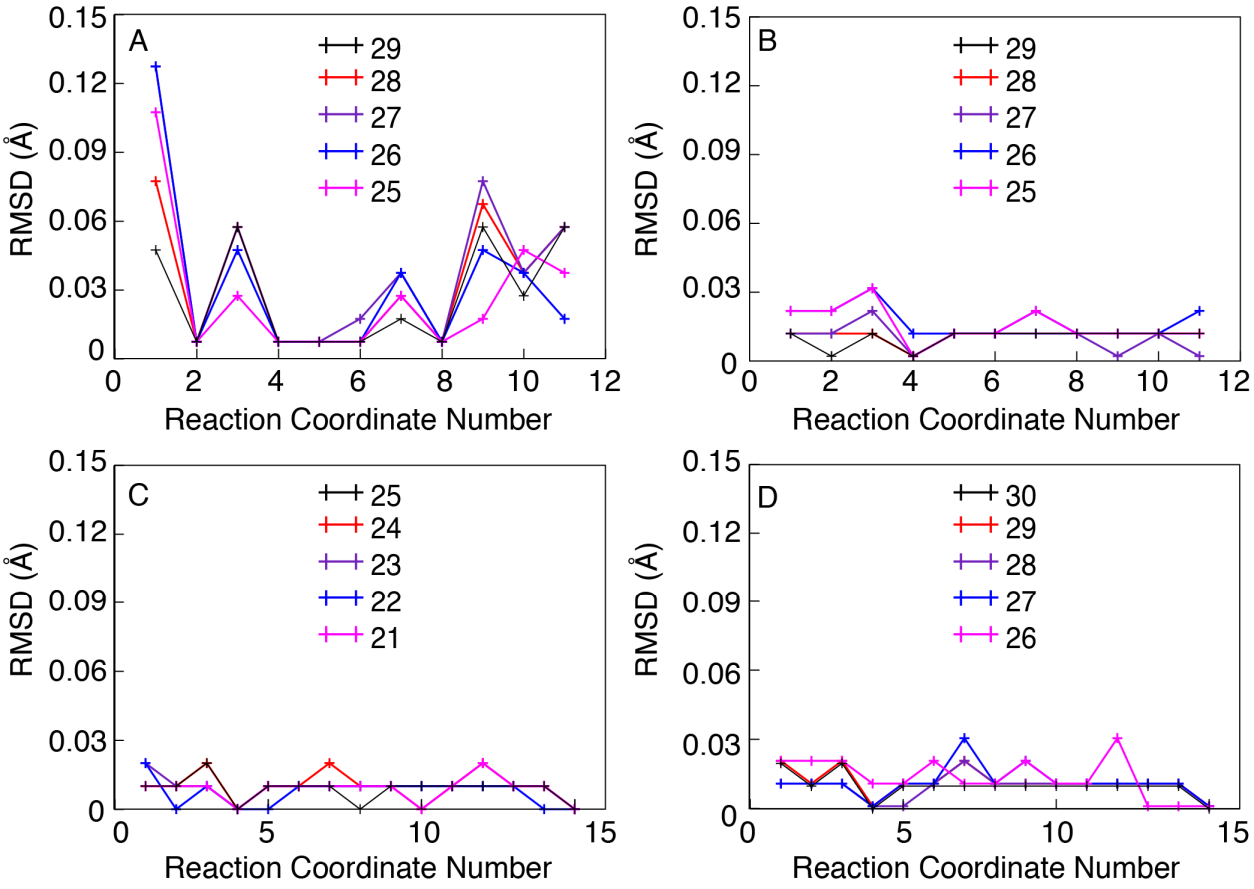

Figure S5: The root-mean-square deviation (RMSD) of each reaction coordinate for the iterations noted in the legend. The RMSD of each reaction coordinate for the specified iteration was calculated relative to its value averaged over the previous five iterations. Parts A and B depict the analyses for the two independent strings of the two-metal system based on the initial strings associated with the sequential and concerted mechanisms, respectively. Parts C and D depict the analyses for the two independent strings of the three-metal system based on the initial strings associated with the sequential and concerted mechanisms, respectively. This figure indicates that the RMSD for all reaction coordinates of all four strings is below 0.1 Å for the final iteration. The RMSDs are somewhat larger for part A than for the other parts because of a slight shifting of the image numbering for the free energy curves in the last few iterations of that string (Figure S6A). However, these RMSD values still meet the convergence criterion described above, and the free energy barriers are fully converged.

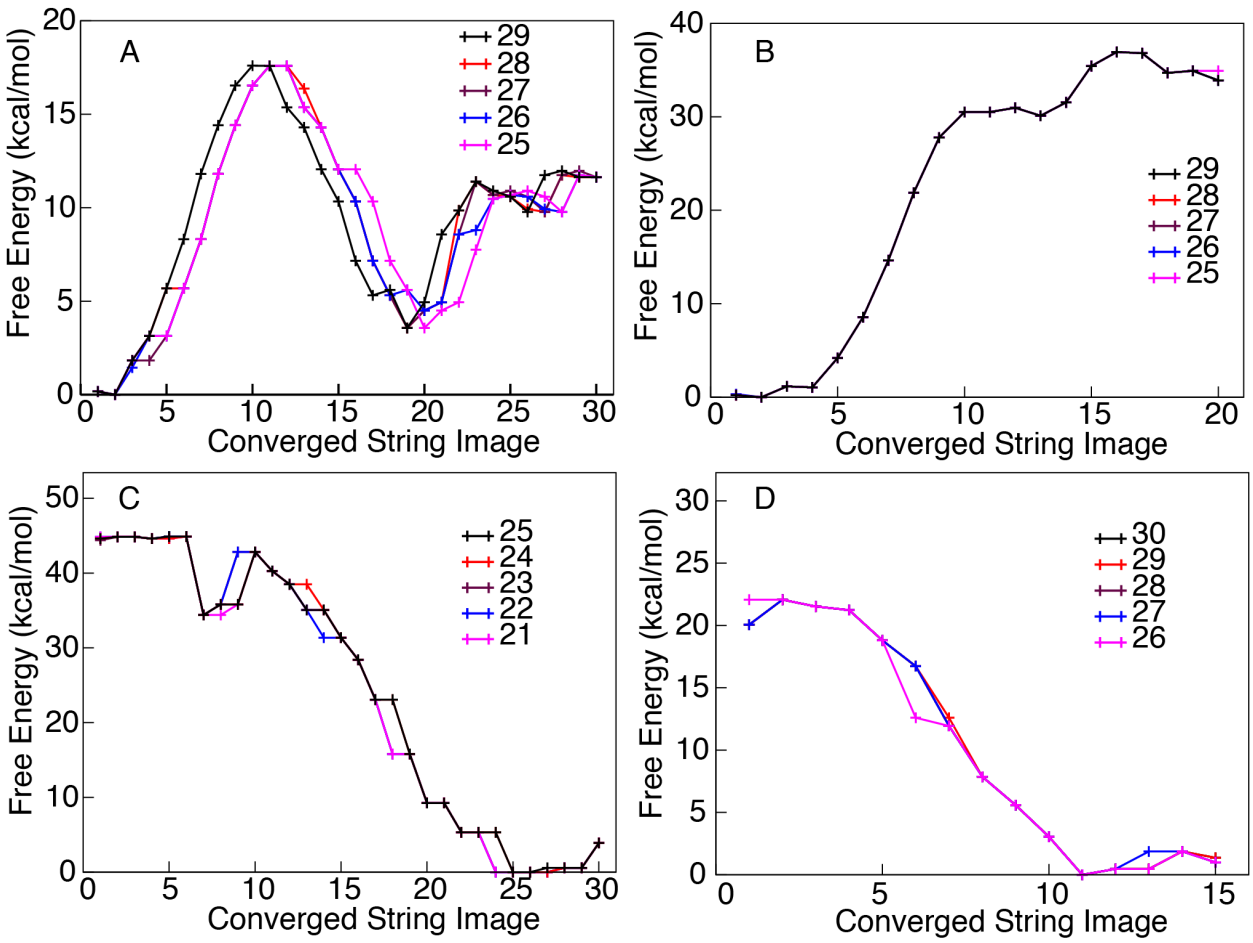

Figure S6: Free energy profiles along the MFEPs for the last five iterations, illustrating convergence of the mechanism and the relative free energies. Parts A and B depict the analyses for the two independent strings of the two-metal system based on the initial strings associated with the sequential and concerted mechanisms, respectively. Parts C and D depict the analyses for the independent strings of the three-metal system based on the initial strings associated with the sequential and concerted mechanisms, respectively. Note that the image numbering is shifted slightly over the last few iterations for part A due to minor slippage of the entire string toward the reactant, but the free energy barriers are converged.

Table S1. Relevant pK_a Values.

System	pKa
Mg-dATP in solution[a]	4.6 γ-phosphate group
dATP in solution[b]	6.53 γ-phosphate group
Aspartatic acid side chain[c]	3.71
Glutamic acid side chain[c]	4.15
H_3O^+ [d]	–1.74
Mg-H_2O in solution[e]	11.2
DNA 3'OH in RNA polymerase with Mn^{2+} [f]	8.2
RNA 2'OH in solution[g]	13.9

[a] Value from Ref. 26; potentiometric pH titrations at 25ºC and I = 0.1M in solution.
[b] Value from Ref. 27; potentiometric pH titrations at 25ºC and I = 0.1M in solution.
[c] Value from Ref. 28.
[d] Value from Ref 29.
[e] Value from Ref. 30; potentiometric pH titrations at 25ºC and I = 0 M in solution.
[f] Value from Ref. 31; pH dependence studies using RNA-dependent RNA polymerase and Mn^{2+}.
[g] Value from Ref. 32; potentiometric pH titration at 10ºC and I = 0.07 M in solution.

Table S2. Hydrogen Bond Analysis for the Two-Metal System in the Reactant State.[a]

Acceptor	Donor	Percentage (%)	Avg. Dist. (Å)	Avg. Angle (°)
ATP O5'	DT3 HO3'	82.5	2.65	155
Water	DT3 HO3'	7.8	2.88	145
ATP O2A	DT3 HO3'	0.9	2.76	150
DT3 O3'	S113 HG	0.1	2.91	163

[a] The classical MD trajectory with protonated 3'OH was propagated for 100 ns. The percentage of the trajectory that the hydrogen bond was present, the average donor-acceptor distance, and the average donor-hydrogen-acceptor angle are given for hydrogen bonds interacting with the attacking oxygen (O3') of thymine. The AMBER program atom nomenclature is used.

Table S3. Hydrogen Bond Analysis for the Three-Metal System in the Reactant State.[a]

Acceptor	Donor	Fraction (%)	Avg. Dist. (Å)	Avg. Angle (°)
ATP O5'	DT3 HO3'	72.7	2.65	152
Water	DT3 HO3'	12.4	2.74	166
ATP O1A	DT3 HO3'	0.1	2.79	145

[a] The classical MD trajectory with protonated 3'OH was propagated for 100 ns. The percentage of the trajectory that the hydrogen bond was present, the average donor-acceptor distance, and the average donor-hydrogen-acceptor angle are given for hydrogen bonds interacting with the attacking oxygen (O3') of thymine. The AMBER program atom nomenclature is used.

Table S4. Hydrogen Bond Analysis for the Two-Metal System in the Reactant State.[a]

Acceptor	Donor	Fraction (%)	Avg. Dist. (Å)	Avg. Angle (°)
ATP O2B	ATP HO3'	99.5	2.65	165
ATP O2G	Y52 HH	96.1	2.60	167
ATP O3G	R55 HH12	88.5	2.79	163
ATP O2G	C16 H	75.0	2.85	165
ATP O3B	R55 HH22	75.0	2.86	158
ATP O2G	K231 HZ1	42.1	2.85	163
ATP O2A	R61 HH22	12.7	2.83	162

[a] The classical MD trajectory with protonated 3'OH was propagated for 100 ns. The percentage of the trajectory that the hydrogen bond was present, the average donor-acceptor distance, and the average donor-hydrogen-acceptor angle are given for hydrogen bonds interacting with the oxygens on the β and γ phosphates of the incoming dATP. The AMBER program atom nomenclature is used.

Table S5. Hydrogen Bond Analysis for the Three-Metal System in the Reactant State.[a]

Acceptor	Donor	Fraction (%)	Avg. Dist. (Å)	Avg. Angle (°)
ATP O2B	ATP HO3'	99.6	2.64	162
ATP O2G	Y52 HH	99.6	2.60	164
ATP O2G	R55 HH22	81.4	2.80	155
ATP O2G	C16 H	59.6	2.86	166
ATP O1B	F17 H	50.4	2.91	158
ATP O2G	R55 HH12	47.6	2.85	149
ATP O2B	R61 HH22	23.9	2.87	152

[a] The classical MD trajectory with protonated 3'OH was propagated for 100 ns. The percentage of the trajectory that the hydrogen bond was present, the average donor-acceptor distance, and the average donor-hydrogen-acceptor angle are given for hydrogen bonds interacting with the oxygens on the β and γ phosphates of the incoming dATP. The AMBER program atom nomenclature is used.

Movie S1. Movie of the QM/MM MD trajectory for the two-metal system demonstrating that a hydroxide ion coordinated to the Mg^{2+} ion in the A position could potentially activate the O3' via deprotonation. The Mg^{2+} ion in the A position is represented by the pink sphere in the foreground. At the beginning of the movie, a hydroxide is bound to the Mg^{2+} ion and is hydrogen bonded to the 3'OH. The Mg^{2+}-bound hydroxide abstracts a proton from O3'H, followed by rotation of the Mg^{2+}-bound water. The total duration of the trajectory is 100 fs.

References

1. Biertumpfel, C.; Zhao, Y.; Kondo, Y.; Ramon-Maiques, S.; Gregory, M.; Lee, J. Y.; Masutani, C.; Lehmann, A. R.; Hanaoka, F.; Yang, W. Structure and mechanism of human DNA polymerase eta. *Nature* **2010,** *465*, 1044-1048.
2. Nakamura, T.; Zhao, Y.; Yamagata, Y.; Hua, Y. J.; Yang, W. Watching DNA polymerase h make a phosphodiester bond. *Nature* **2012,** *487*, 196-201.
3. Schrödinger, L., Schrödinger Release 2017-4: Maestro. **2017**.
4. Gordon, J. C.; Myers, J. B.; Folta, T.; Shoja, V.; Heath, L. S.; Onufriev, A. H++: a server for estimating pK(a)s and adding missing hydrogens to macromolecules. *Nucleic Acids Res.* **2005,** *33*, W368-W371.
5. Jorgensen, W. L.; Chandrasekhar, J.; Madura, J. D.; Impey, R. W.; Klein, M. L. Comparison of simple potential functions for simulating liquid water. *J. Chem. Phys.* **1983,** *79*, 926-935.
6. Cornell, W. D.; Cieplak, P.; Bayly, C. I.; Gould, I. R.; Merz, K. M.; Ferguson, D. M.; Spellmeyer, D. C.; Fox, T.; Caldwell, J. W.; Kollman, P. A. A Second Generation Force Field for the Simulation of Proteins, Nucleic Acids, and Organic Molecules. *J. Am. Chem. Soc.* **1995,** *117*, 5179-5197.
7. Cheatham, T. E.; Cieplak, P.; Kollman, P. A. A Modified Version of the Cornell et al. Force Field with Improved Sugar Pucker Phases and Helical Repeat. *J. Biomol. Struct. Dyn.* **1999,** *16*, 845-862.
8. Hornak, V.; Abel, R.; Okur, A.; Strockbine, B.; Roitberg, A.; Simmerling, C. Comparison of multiple Amber force fields and development of improved protein backbone parameters. *Proteins* **2006,** *65*, 712-725.
9. Pérez, A.; Marchán, I.; Svozil, D.; Sponer, J.; Cheatham, T. E.; Laughton, C. A.; Orozco, M. Refinement of the AMBER Force Field for Nucleic Acids: Improving the Description of α/γ Conformers. *Biophys. J.* **2007,** *92*, 3817-3829.
10. Maier, J. A.; Martinez, C.; Kasavajhala, K.; Wickstrom, L.; Hauser, K. E.; Simmerling, C., ff14SB: Improving the Accuracy of Protein Side Chain and Backbone Parameters from ff99SB. *J. Chem. Theory Comput.* **2015,** *11*, 3696-3713.
11. Yang, Y.; Miao, Y.; Wang, B.; Cui, G.; Merz, K. M., Jr. Catalytic mechanism of aromatic prenylation by NphB. *Biochemistry* **2012,** *51*, 2606-18.
12. Ucisik, M. N.; Hammes-Schiffer, S. Comparative Molecular Dynamics Studies of Human DNA Polymerase h. *J. Chem. Inf. Model.* **2015,** *55*, 2672-81.
13. Case, D. A.; Cheatham, T. E., 3rd; Darden, T.; Gohlke, H.; Luo, R.; Merz, K. M., Jr.; Onufriev, A.; Simmerling, C.; Wang, B.; Woods, R. J. The Amber biomolecular simulation programs. *J. Comput. Chem.* **2005,** *26*, 1668-88.
14. D.A. Case, J.T. Berryman, R.M. Betz, D.S. Cerutti, T.E. Cheatham, III, T.A. Darden, R.E. Duke, T.J. Giese, H. Gohlke, A.W. Goetz, N. Homeyer, S. Izadi, P. Janowski, J. Kaus, A. Kovalenko, T.S. Lee, S. LeGrand, P. Li, T. Luchko, R. Luo, B. Madej, K.M. Merz, G. Monard, P. Needham, H. Nguyen, H.T. Nguyen, I. Omelyan, A. Onufriev, D.R. Roe, A. Roitberg, R. Salomon-Ferrer, C.L. Simmerling, W. Smith, J. Swails, R.C. Walker, J. Wang, R.M. Wolf, X. Wu, D.M. York and P.A. Kollman *AMBER 2015*, University of California, San Francisco.: 2015.

15. Brooks, B. R.; Brooks, C. L., 3rd; Mackerell, A. D., Jr.; Nilsson, L.; Petrella, R. J.; Roux, B.; Won, Y.; Archontis, G.; Bartels, C.; Boresch, S.; Caflisch, A.; Caves, L.; Cui, Q.; Dinner, A. R.; Feig, M.; Fischer, S.; Gao, J.; Hodoscek, M.; Im, W.; Kuczera, K.; Lazaridis, T.; Ma, J.; Ovchinnikov, V.; Paci, E.; Pastor, R. W.; Post, C. B.; Pu, J. Z.; Schaefer, M.; Tidor, B.; Venable, R. M.; Woodcock, H. L.; Wu, X.; Yang, W.; York, D. M.; Karplus, M. CHARMM: the Biomolecular Simulation Program. *J. Comput. Chem.* **2009,** *30*, 1545-614.
16. Shao, Y.; Molnar, L. F.; Jung, Y.; Kussmann, J.; Ochsenfeld, C.; Brown, S. T.; Gilbert, A. T. B.; Slipchenko, L. V.; Levchenko, S. V.; O'Neill, D. P.; DiStasio, R. A.; Lochan, R. C.; Wang, T.; Beran, G. J. O.; Besley, N. A.; Herbert, J. M.; Lin, C. Y.; Van Voorhis, T.; Chien, S. H.; Sodt, A.; Steele, R. P.; Rassolov, V. A.; Maslen, P. E.; Korambath, P. P.; Adamson, R. D.; Austin, B.; Baker, J.; Byrd, E. F. C.; Dachsel, H.; Doerksen, R. J.; Dreuw, A.; Dunietz, B. D.; Dutoi, A. D.; Furlani, T. R.; Gwaltney, S. R.; Heyden, A.; Hirata, S.; Hsu, C. P.; Kedziora, G.; Khalliulin, R. Z.; Klunzinger, P.; Lee, A. M.; Lee, M. S.; Liang, W.; Lotan, I.; Nair, N.; Peters, B.; Proynov, E. I.; Pieniazek, P. A.; Rhee, Y. M.; Ritchie, J.; Rosta, E.; Sherrill, C. D.; Simmonett, A. C.; Subotnik, J. E.; Woodcock, H. L.; Zhang, W.; Bell, A. T.; Chakraborty, A. K.; Chipman, D. M.; Keil, F. J.; Warshel, A.; Hehre, W. J.; Schaefer, H. F.; Kong, J.; Krylov, A. I.; Gill, P. M. W.; Head-Gordon, M. Advances in methods and algorithms in a modern quantum chemistry program package. *Phys. Chem. Chem. Phys.* **2006,** *8*, 3172-3191.
17. Woodcock, H. L., 3rd; Hodoscek, M.; Gilbert, A. T.; Gill, P. M.; Schaefer, H. F., 3rd; Brooks, B. R. Interfacing Q-Chem and CHARMM to perform QM/MM reaction path calculations. *J. Comput. Chem.* **2007,** *28*, 1485-502.
18. Lee, C.; Yang, W.; Parr, R. G., Development of the Colle-Salvetti correlation-energy formula into a functional of the electron density. *Phys. Rev. B. Condens. Matter* **1988,** *37*, 785-789.
19. Becke, A. D., Density-functional thermochemistry. III. The role of exact exchange. *J. Chem. Phys.* **1993,** *98*, 5648-5652.
20. Rosta, E.; Nowotny, M.; Yang, W.; Hummer, G. Catalytic Mechanism of RNA Backbone Cleavage by Ribonuclease H from Quantum Mechanics/Molecular Mechanics Simulations. *J. Am. Chem. Soc.* **2011,** *133*, 8934-41.
21. Ganguly, A.; Thaplyal, P.; Rosta, E.; Bevilacqua, P. C.; Hammes-Schiffer, S. Quantum Mechanical/Molecular Mechanical Free Energy Simulations of the Self-Cleavage Reaction in the Hepatitis Delta Virus Ribozyme. *J. Am. Chem. Soc.* **2014,** *136*, 1483-1496.
22. Zhang, S.; Ganguly, A.; Goyal, P.; Bingaman, J. L.; Bevilacqua, P. C.; Hammes-Schiffer, S. Role of the Active Site Guanine in the *glmS* Ribozyme Self-Cleavage Mechanism: Quantum Mechanical/Molecular Mechanical Free Energy Simulations. *J. Am. Chem. Soc.* **2015,** *137*, 784-98.
23. Li, P.; Soudackov, A. V.; Hammes-Schiffer, S. Fundamental Insights into Proton-Coupled Electron Transfer in Soybean Lipoxygenase from Quantum Mechanical/Molecular Mechanical Free Energy Simulations. *J. Am. Chem. Soc.* **2018**.
24. Souaille, M.; Roux, B. T. Extension to the weighted histogram analysis method: combining umbrella sampling with free energy calculations. *Comput. Phys. Commun.* **2001,** *135*, 40-57.
25. Grossfield, A., WHAM: the weighted histogram analysis method. *WHAM version 2.0.9*.
26. Sigel, H.; Griesser, R., Nucleoside 5'-triphosphates: self-association, acid-base, and metal ion-binding properties in solution. *Chem. Soc. Rev.* **2005,** *34*, 875-900

27. Taqui Khan, M. M.; Martell, A. E., Thermodynamic Quantities Associated with the Interaction of Adenosine Triphosphate with Metal Ions1,2. *J. Am. Chem. Soc.* **1966,** *88*, 668-671.
28. David R. Lide, ed., *CRC Handbook of Chemistry and Physics, Internet Version 2005*, CRC Press, Boca Raton, FL, 2005
29. Ikeda, T.; Saito, K.; Hasegawa, R.; Ishikita, H., The Existence of an Isolated Hydronium Ion in the Interior of Proteins. *Angew. Chem. Int. Ed. Engl.* **2017,** *56*, 9151-9154.
30. Grzybkowski, W., Nature and properties of metal cations in aqueous solutions. *Pol. J. Env. Stud.* **2006,** *15*
31. Castro, C.; Smidansky, E.; Maksimchuk, K. R.; Arnold, J. J.; Korneeva, V. S.; Gotte, M.; Konigsberg, W.; Cameron, C. E., Two proton transfers in the transition state for nucleotidyl transfer catalyzed by RNA- and DNA-dependent RNA and DNA polymerases. *Proc. Natl. Acad. Sci. U.S.A.* **2007,** *104*, 4267-72.
32. Usher, D. A.; Richardson, D. I.; Oakenfull, D. G., Models of ribonuclease action. II. Specific acid, specific base, and neutral pathways for hydrolysis of a nucleotide diester analog. *J. Am. Chem. Soc.* **1970,** *92*, 4699-4712.